Available online at www.sciencedirect.com
ScienceDirect
Physics Letters B 654 (2007) 65–73
PHYSICS LETTERS B
www.elsevier.com/locate/physletb

Study of $\tau^- \to K_S \pi^- \nu_\tau$ decay at Belle

Belle Collaboration

D. Epifanov [a,*], I. Adachi [g], H. Aihara [ar], K. Arinstein [a], V. Aulchenko [a], T. Aushev [q,l], A.M. Bakich [am], V. Balagura [l], E. Barberio [t], I. Bedny [a], K. Belous [j], U. Bitenc [m], I. Bizjak [m], A. Bondar [a], A. Bozek [z], M. Bračko [s,m], T.E. Browder [f], Y. Chao [y], A. Chen [w], K.-F. Chen [y], W.T. Chen [w], B.G. Cheon [e], C.-C. Chiang [y], R. Chistov [l], I.-S. Cho [av], Y. Choi [al], Y.K. Choi [al], J. Dalseno [t], M. Dash [au], A. Drutskoy [c], S. Eidelman [a], G. Gokhroo [an], B. Golob [r,m], H. Ha [o], J. Haba [g], K. Hayasaka [u], H. Hayashii [v], M. Hazumi [g], D. Heffernan [ae], T. Hokuue [u], Y. Hoshi [ap], W.-S. Hou [y], Y.B. Hsiung [y], H.J. Hyun [p], T. Iijima [u], K. Ikado [u], K. Inami [u], A. Ishikawa [ar], R. Itoh [g], M. Iwasaki [ar], Y. Iwasaki [g], D.H. Kah [p], H. Kaji [u], J.H. Kang [av], H. Kawai [b], T. Kawasaki [ab], H. Kichimi [g], H.O. Kim [al], S.K. Kim [ak], Y.J. Kim [d], P. Križan [r,m], P. Krokovny [g], R. Kumar [af], C.C. Kuo [w], A. Kuzmin [a], Y.-J. Kwon [av], J.S. Lee [al], M.J. Lee [ak], S.E. Lee [ak], T. Lesiak [z], J. Li [f], A. Limosani [t], S.-W. Lin [y], Y. Liu [d], D. Liventsev [l], F. Mandl [k], D. Marlow [ah], T. Matsumoto [as], A. Matyja [z], S. McOnie [am], T. Medvedeva [l], H. Miyata [ab], Y. Miyazaki [u], R. Mizuk [l], G.R. Moloney [t], T. Mori [u], E. Nakano [ad], M. Nakao [g], H. Nakazawa [w], Z. Natkaniec [z], S. Nishida [g], O. Nitoh [at], S. Ogawa [ao], T. Ohshima [u], Y. Onuki [ai], W. Ostrowicz [z], H. Ozaki [g], P. Pakhlov [l], G. Pakhlova [l], H. Palka [z], C.W. Park [al], H. Park [p], K.S. Park [al], L.S. Peak [am], R. Pestotnik [m], L.E. Piilonen [au], A. Poluektov [a], H. Sahoo [f], Y. Sakai [g], O. Schneider [q], R. Seidl [h,ai], K. Senyo [u], M.E. Sevior [t], M. Shapkin [j], H. Shibuya [ao], B. Shwartz [a], A. Sokolov [j], A. Somov [c], N. Soni [af], S. Stanič [ac], M. Starič [m], H. Stoeck [am], T. Sumiyoshi [as], F. Takasaki [g], K. Tamai [g], M. Tanaka [g], G.N. Taylor [t], Y. Teramoto [ad], X.C. Tian [ag], I. Tikhomirov [l], T. Tsuboyama [g], S. Uehara [g], K. Ueno [y], T. Uglov [l], Y. Unno [e], S. Uno [g], P. Urquijo [t], Y. Usov [a], G. Varner [f], K. Vervink [q], S. Villa [q], A. Vinokurova [a], C.H. Wang [x], P. Wang [i], Y. Watanabe [n], R. Wedd [t], E. Won [o], B.D. Yabsley [am], A. Yamaguchi [aq], Y. Yamashita [aa], M. Yamauchi [g], C.Z. Yuan [i], Z.P. Zhang [aj], V. Zhilich [a], A. Zupanc [m]

[a] *Budker Institute of Nuclear Physics, Novosibirsk, Russia*
[b] *Chiba University, Chiba, Japan*
[c] *University of Cincinnati, Cincinnati, OH, USA*
[d] *The Graduate University for Advanced Studies, Hayama, Japan*
[e] *Hanyang University, Seoul, South Korea*
[f] *University of Hawaii, Honolulu, HI, USA*
[g] *High Energy Accelerator Research Organization (KEK), Tsukuba, Japan*
[h] *University of Illinois at Urbana-Champaign, Urbana, IL, USA*
[i] *Institute of High Energy Physics, Chinese Academy of Sciences, Beijing, PR China*
[j] *Institute for High Energy Physics, Protvino, Russia*
[k] *Institute of High Energy Physics, Vienna, Austria*
[l] *Institute for Theoretical and Experimental Physics, Moscow, Russia*
[m] *J. Stefan Institute, Ljubljana, Slovenia*
[n] *Kanagawa University, Yokohama, Japan*
[o] *Korea University, Seoul, South Korea*
[p] *Kyungpook National University, Taegu, South Korea*
[q] *Swiss Federal Institute of Technology of Lausanne, EPFL, Lausanne, Switzerland*
[r] *University of Ljubljana, Ljubljana, Slovenia*

0370-2693/$ – see front matter © 2007 Elsevier B.V. All rights reserved.
doi:10.1016/j.physletb.2007.08.045

[s] University of Maribor, Maribor, Slovenia
[t] University of Melbourne, Victoria, Australia
[u] Nagoya University, Nagoya, Japan
[v] Nara Women's University, Nara, Japan
[w] National Central University, Chung-li, Taiwan
[x] National United University, Miao Li, Taiwan
[y] Department of Physics, National Taiwan University, Taipei, Taiwan
[z] H. Niewodniczanski Institute of Nuclear Physics, Krakow, Poland
[aa] Nippon Dental University, Niigata, Japan
[ab] Niigata University, Niigata, Japan
[ac] University of Nova Gorica, Nova Gorica, Slovenia
[ad] Osaka City University, Osaka, Japan
[ae] Osaka University, Osaka, Japan
[af] Panjab University, Chandigarh, India
[ag] Peking University, Beijing, PR China
[ah] Princeton University, Princeton, NJ, USA
[ai] RIKEN BNL Research Center, Brookhaven, NY, USA
[aj] University of Science and Technology of China, Hefei, PR China
[ak] Seoul National University, Seoul, South Korea
[al] Sungkyunkwan University, Suwon, South Korea
[am] University of Sydney, Sydney, NSW, Australia
[an] Tata Institute of Fundamental Research, Mumbai, India
[ao] Toho University, Funabashi, Japan
[ap] Tohoku Gakuin University, Tagajo, Japan
[aq] Tohoku University, Sendai, Japan
[ar] Department of Physics, University of Tokyo, Tokyo, Japan
[as] Tokyo Metropolitan University, Tokyo, Japan
[at] Tokyo University of Agriculture and Technology, Tokyo, Japan
[au] Virginia Polytechnic Institute and State University, Blacksburg, VA, USA
[av] Yonsei University, Seoul, South Korea

Received 15 June 2007; accepted 13 August 2007

Available online 29 August 2007

Editor: M. Doser

Abstract

We present a study of the decay $\tau^- \to K_S\pi^-\nu_\tau$ using a 351 fb^{-1} data sample collected with the Belle detector. The analysis is based on 53, 110 lepton-tagged signal events. The measured branching fraction $\mathcal{B}(\tau^- \to K_S\pi^-\nu_\tau) = (0.404 \pm 0.002(\text{stat.}) \pm 0.013(\text{syst.}))\%$ is consistent with the world average value and has better accuracy. An analysis of the $K_S\pi^-$ invariant mass spectrum reveals contributions from the $K^*(892)^-$ as well as other states. For the first time the $K^*(892)^-$ mass and width have been measured in τ decay: $M(K^*(892)^-) = (895.47 \pm 0.20(\text{stat.}) \pm 0.44(\text{syst.}) \pm 0.59(\text{mod.}))$ MeV/c^2, $\Gamma(K^*(892)^-) = (46.2 \pm 0.6(\text{stat.}) \pm 1.0(\text{syst.}) \pm 0.7(\text{mod.}))$ MeV. The $K^*(892)^-$ mass is significantly different from the current world average value.
© 2007 Elsevier B.V. All rights reserved.

PACS: 13.30.Eg; 13.35.Dx; 13.66.Jn; 14.40.Ev; 14.60.Fg

Keywords: Tau; K^*

1. Introduction

τ lepton hadronic decays provide a laboratory for the study of low energy hadronic currents under very clean conditions. In these decays, the hadronic system is produced from the QCD vacuum via the charged weak current mediated by a $W^\pm$ boson. The τ decay amplitude can thus be factorized into a purely leptonic part including the τ and ν_τ and a hadronic spectral function. Strangeness changing τ decays are suppressed by a factor of $\simeq 20$ relative to Cabibbo-allowed modes. High-statistics measurements at B factories provide excellent opportunities for studying the structure of the strange hadronic spectral functions in specific decay modes [1–3], the parameters of the intermediate states and the total strange hadronic spectral function [4].

The decay $\tau^- \to \bar{K}^0\pi^-\nu_\tau$ (unless specified otherwise, charge conjugate decays are implied throughout the Letter) has the largest branching fraction of all Cabibbo-suppressed decays of the τ lepton. Early studies of this decay established that the main contribution to the $K\pi$ invariant mass spectrum is from the $K^*(892)$ meson [5–7]. Although scalar or tensor contributions are expected in theoretical models [8,9] and not excluded experimentally [10,11], the low statistics of previous investigations did not allow for a detailed study.

* Corresponding author.
E-mail address: d.a.epifanov@inp.nsk.su (D. Epifanov).

Here we report a precise measurement of the branching fraction for the decay $\tau^- \to K_S\pi^-\nu_\tau$ as well as a study of its final state dynamics. This analysis is based on a 351 fb^{-1} data sample that contains $313 \times 10^6 \tau^+\tau^-$ pairs, collected with the Belle detector at the KEKB energy-asymmetric e^+e^- (3.5 on 8 GeV) collider [12] operating at the $\Upsilon(4S)$ resonance.

2. The Belle detector

The Belle detector is a large-solid-angle magnetic spectrometer that consists of a silicon vertex detector (SVD), a 50-layer central drift chamber (CDC), an array of aerogel threshold Cherenkov counters (ACC), a barrel-like arrangement of time-of-flight scintillation counters (TOF), and an electromagnetic calorimeter (ECL) comprised of CsI(Tl) crystals located inside a superconducting solenoid coil that provides a 1.5 T magnetic field. An iron flux-return located outside the coil is instrumented to detect K_L^0 mesons and to identify muons (KLM). Two inner detector configurations are used in this analysis. A beampipe with a radius of 2.0 cm and a 3-layer silicon vertex detector are used for the first sample of $124 \times 10^6 \tau^+\tau^-$ pairs, while a 1.5 cm beampipe, a 4-layer silicon detector and a small-cell inner drift chamber are used to record the remaining $189 \times 10^6 \tau^+\tau^-$ pairs [13]. The detector is described in detail elsewhere [14].

3. Selection of $\tau^+\tau^-$ events

We select events in which one τ decays to leptons, $\tau^- \to l^-\bar{\nu}_l\nu_\tau$, $l = e, \mu$, while the other one decays via the hadronic channel $\tau^- \to h^-\nu_\tau$, where h^- denotes the hadronic system. Events where both τ's decay to leptons are used for normalization. This reduces systematic uncertainties substantially.

The selection process, which is optimized to suppress background while retaining a high efficiency for the decays under study, proceeds in two stages. The criteria of the first stage suppress beam background to a negligible level and reject most of the background from other physical processes. These criteria retain a 46.0% efficiency for $\tau^+\tau^-$ events. We then select events having 2 to 4 tracks with a net charge less than or equal to one in absolute value. The extrapolation of each track to the interaction point (IP) is required to pass within ± 0.5 cm in the transverse direction and ± 2.5 cm in the longitudinal direction of the nominal collision point of the beams. Each track must have a transverse momentum in the center-of-mass (CM) frame larger than 0.1 GeV/c. At least one of the charged particles should have a transverse momentum higher than 0.5 GeV/c. The sum of the absolute values of the CM track momenta must be less than 9 GeV/c. The minimum opening angle for any pair of tracks is required to be larger than 20°. The number of photons with a CM energy exceeding 80 MeV is required to be less than or equal to five. The total ECL energy deposition in the laboratory frame must be less than 9 GeV. The total energy of all photon candidates in the laboratory frame should satisfy $\sum E_\gamma^{\rm LAB} < 0.2$ GeV. The missing four-momentum $P_{\rm miss}$ is calculated by subtracting the four-momentum of all charged tracks and photons from the beam four-momentum. The missing mass $M_{\rm miss} = \sqrt{P_{\rm miss}^2}$ is required to satisfy 1 GeV/$c^2 \leqslant M_{\rm miss} \leqslant 7$ GeV/c^2. The polar angle of the missing momentum in the CM frame is required to be larger than or equal to 30° and less than or equal to 150°. The last two criteria are particularly effective in suppressing the backgrounds from radiative Bhabha, $e^+e^- \to \mu^+\mu^-(\gamma)$ and two-photon processes.

At the second stage, two event classes are selected for further processing: a two-lepton sample $(l_1^\pm, l_2^\mp)$, $l_1, l_2 = e, \mu$ and a lepton–hadron sample $(l^\pm, K_S\pi^\mp)$, $l = e, \mu$. To select electrons, a likelihood ratio requirement $\mathcal{P}_e = \mathcal{L}_e/(\mathcal{L}_e + \mathcal{L}_x) > 0.8$ is applied, where the electron likelihood function $\mathcal{L}_e$ and the non-electron function $\mathcal{L}_x$ include information on the specific ionization (dE/dx) measurement by the CDC, the ratio of the cluster energy in the ECL to the track momentum measured in the CDC, the transverse ECL shower shape and the light yield in the ACC [15]. The efficiency of this requirement for electrons is 93%. To select muons, a likelihood ratio requirement $\mathcal{P}_\mu = \mathcal{L}_\mu/(\mathcal{L}_\mu + \mathcal{L}_\pi + \mathcal{L}_K) > 0.8$ is applied. It provides 88% efficiency for muons. Each of the muon ($\mathcal{L}_\mu$), pion ($\mathcal{L}_\pi$) and kaon ($\mathcal{L}_K$) likelihood functions is evaluated from the information on the difference between the range calculated from the momentum of the particle and the range measured by KLM, and the χ^2 of the KLM hits with respect to the extrapolated track [16]. To separate pions from kaons, for each track we determine the pion ($\mathcal{L}'_\pi$) and kaon ($\mathcal{L}'_K$) likelihoods from the ACC response, the dE/dx measurement in the CDC and the TOF flight-time measurement, and form a likelihood ratio $\mathcal{P}_{K/\pi} = \mathcal{L}'_K/(\mathcal{L}'_\pi + \mathcal{L}'_K)$. For pions we apply the requirement $\mathcal{P}_{K/\pi} < 0.3$, which provides a pion identification efficiency of about 93%, while keeping the pion fake rate at the 6% level.

To evaluate the background and to calculate efficiencies, a Monte Carlo (MC) sample of $1.50 \times 10^9 \tau^+\tau^-$ pairs is produced with the KORALB/TAUOLA generators [17,18]. The detector response is simulated by a GEANT3 based program [19].

3.1. Two–lepton events

For this class the (e, e) and (μ, μ) samples still contain contamination from radiative Bhabha and $e^+e^- \to \mu^+\mu^-(\gamma)$ processes of about 50%, only (e, μ) events are used for normalization. To further suppress $B\bar{B}$ and charm backgrounds, we require the opening angle of the leptons to be larger than 90° in the CM. As a result, we selected 2 018 000 events of the (e^+, μ^-) type and 2 028 000 (e^-, μ^+) events.

MC simulation indicates that there is an approximately 5% contamination coming primarily from the two-photon process $e^+e^- \to e^+e^-\mu^+\mu^-$ (2.0%) and from $\tau^+\tau^- \to e^+(\mu^+)\pi^-\nu_e(\nu_\mu)\nu_\tau\bar{\nu}_\tau$ events where the π is misidentified as a lepton (2.8%). Contamination from other non-$\tau^+\tau^-$ processes is found to be negligible (less than 0.1%). The numbers of (e^+, μ^-) and (e^-, μ^+) events after background subtraction are $1\,929\,300 \pm 1\,400$ and $1\,911\,700 \pm 1\,400$, respectively. The detection efficiencies and their statistical errors are $(19.262 \pm 0.006)\%$ for (e^+, μ^-) and $(19.252 \pm 0.006)\%$ for (e^-, μ^+) events.

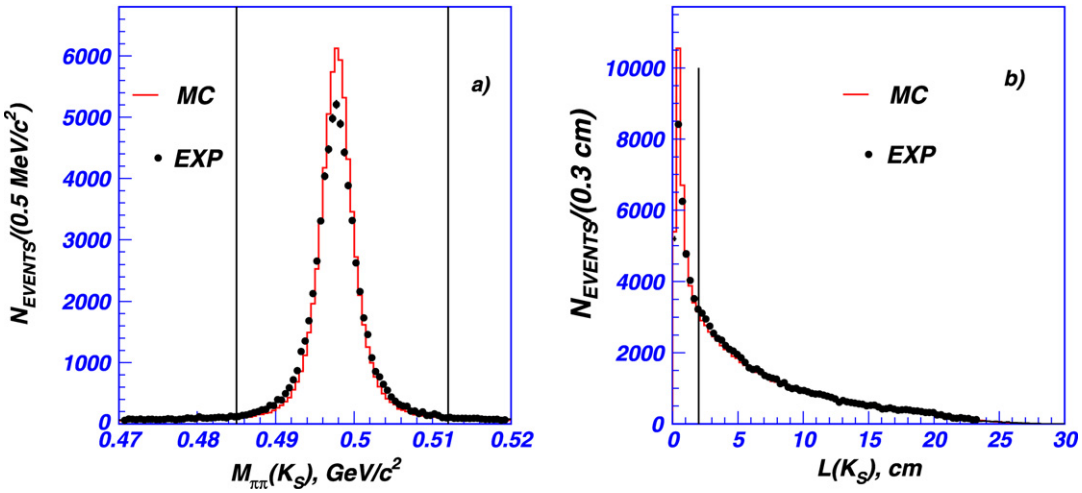

Fig. 1. MC (histogram) and experimental data (points) distributions normalized to the same number of events. (a) shows the $\pi^+\pi^-$ invariant mass distribution for K_S candidates. (b) shows the K_S candidate decay length. For each distribution all the criteria described in the text except the one pertaining to the displayed parameter are applied. Applied cuts are shown by vertical lines.

3.2. Lepton–hadron events

For this class we select events with only one lepton $l^\pm$ ($l = e, \mu$), one K_S candidate and one charged pion $\pi^\mp$. A K_S meson is reconstructed from a pair of oppositely charged pions having invariant mass $M_{\pi\pi}(K_S)$ within ± 13.5 MeV of the K_S mass, which corresponds to a $\pm 5\sigma$ signal range. The pion momenta are then refitted with a common vertex constraint. The z-distance between the two helices at the $\pi^+\pi^-$ vertex position before the fit is required to be less than 1.5 cm, where z is defined as the direction opposite to the positron beam. The closest approach of at least one track to the IP in the r–φ plane must be larger than 0.03 cm. The decay length of the K_S candidate in the r–φ plane must satisfy $0.1\ \text{cm} \leqslant L_\perp \leqslant 20\ \text{cm}$. The z-projection of the K_S candidate decay length is required to be $L_z \leqslant 20$ cm. The K_S decay length $L(K_S) = \sqrt{L_\perp^2 + L_z^2}$ must be larger than 2 cm. The cosine of the azimuthal angle between the momentum vector and the decay vertex vector of the K_S candidate is required to be larger than or equal to 0.95. The lepton-K_S and lepton-π opening angles are required to be larger than 90^o in the CM. 68, 107 events were selected for further analysis. Fig. 1 shows a comparison of the MC and experimental distributions for the $\pi^+\pi^-$ invariant mass of the K_S candidate and the K_S decay length.

Fig. 1(a) shows that MC $\pi^+\pi^-$ mass resolution is slightly better than the experimental one resulting in a clear difference of the $\pi^+\pi^-$ mass spectra in the region of the K_S peak. However, the efficiency of the $M_{\pi\pi}$ cut for the K_S candidates is almost 100%, hence the impact of this discrepancy on the detection efficiency is very small and is taken into account in the systematic uncertainty. In Fig. 1(b) one can see a clear difference between the $L(K_S)$ distributions in the region of small $L(K_S)$, where events of $\tau^- \to \pi^-\pi^-\pi^+\nu_\tau$ decay are located, however, in the region, where $L(K_S) > 2$ cm, populated mostly by true K_S's the agreement is good. Fig. 2 shows selected events on a plot of the K_S decay length versus the $\pi^+\pi^-$ invariant mass of the K_S candidate. The main background is from other τ decays: $\tau^- \to K_S\pi^- K_L\nu_\tau$, $\tau^- \to K_S\pi^-\pi^0\nu_\tau$, $\tau^- \to K_S K^-\nu_\tau$, $\tau^- \to \pi^-\pi^-\pi^+\nu_\tau$. Using the branching fractions of these decays from Ref. [20] and detection efficiencies from MC simulation, the contamination from decays with a K_S is calculated to be 14.7%. $\tau^- \to \pi^-\pi^-\pi^+\nu_\tau$ decays contaminate the sample when a pair of oppositely charged pions is reconstructed as a fake K_S. The $\pi^+\pi^-$ invariant mass distribution of these fake K_S's is flat in the region of the K_S mass (see also Fig. 2). The number of 3π background events is calculated from two sideband regions in the $L(K_S)$ vs $M_{\pi\pi}(K_S)$ plane, determined by the following criteria: $468\ \text{MeV}/c^2 < M_{\pi\pi}(K_S) < 482\ \text{MeV}/c^2$ and $L(K_S) > 2$ cm for the first region, $515\ \text{MeV}/c^2 < M_{\pi\pi}(K_S) < 528\ \text{MeV}/c^2$ and $L(K_S) > 2$ cm for the second one. These sidebands have the same area as the signal region. From MC simulation the fraction of signal events in the sideband region is found to be about 1%, which is taken into account in the calculation of the MC signal detection efficiency. We have a 5.6% background of 3π events in the signal region. MC simulation indicates that in the $(l^\pm, K_S\pi^\mp)$, $l = e, \mu$ sample there is a small contamination (of about 0.3% for the e-tagged and 2.4% for the μ-tagged events) coming primarily from $(\pi^\pm, K_S\pi^\mp)$ events, where the first pion was misidentified as a lepton. As it is found from MC simulation the non-$\tau^+\tau^-$ background is about 0.6%. After background subtraction $53\,110 \pm 271$ signal events remain. Table 1 shows how they are distributed among the various tagging configurations.

4. $\tau^- \to K_S\pi^-\nu_\tau$ branching fraction

The $\tau^- \to K_S\pi^-\nu_\tau$ branching fraction is calculated according to the formula:

$$\mathcal{B}(K_S\pi^\mp\nu_\tau) = \frac{N(l_1^\pm, K_S\pi^\mp)}{N(l_1^\pm, l_2^\mp)} \cdot \frac{\varepsilon(l_1^\pm, l_2^\mp)}{\varepsilon(l_1^\pm, K_S\pi^\mp)} \cdot \mathcal{B}(l_2^\mp\nu_l\nu_\tau), \quad l_{1,2} = e, \mu, \tag{1}$$

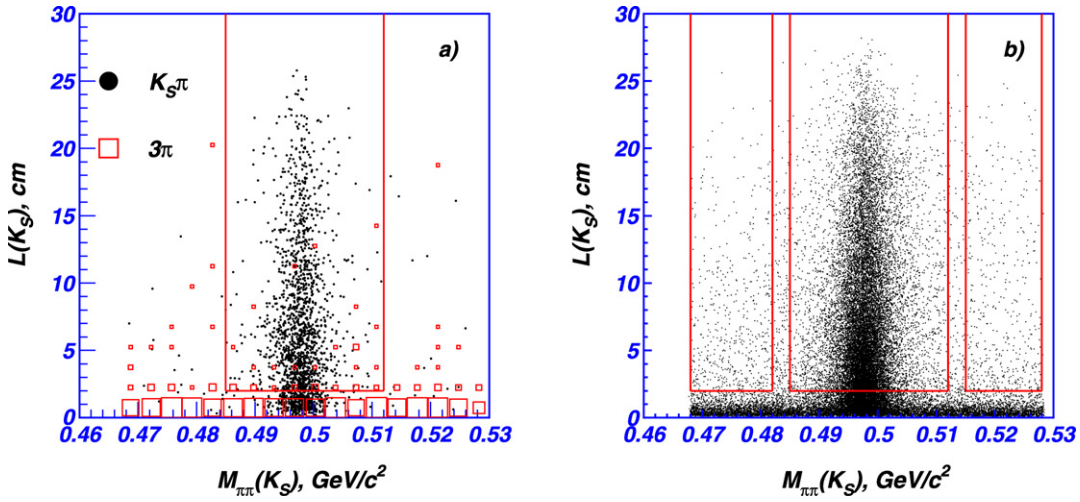

Fig. 2. Decay length vs $\pi\pi$ invariant mass of the K_S candidate for $(e^+, K_S\pi^-)$ events. All selection criteria described in the text except for those pertaining to the parameters being displayed are applied. (a) Shows MC data, where events with a real K_S are plotted as points, and the events with fake K_S's from $\tau^- \to \pi^+\pi^-\pi^-\nu_\tau$ are plotted as boxes, whose sizes are proportional to the number of entries. (b) Shows experimental data. The signal region is indicated by the middle rectangle, while sideband regions are shown by the rectangles to the left and right of the signal region.

Table 1
Branching fractions for different tagging configurations

	$(e^+, K_S\pi^-)$	$(e^-, K_S\pi^+)$	$(\mu^+, K_S\pi^-)$	$(\mu^-, K_S\pi^+)$
$N_{\rm exp}$	13336 ± 137	13308 ± 137	13230 ± 134	13236 ± 134
$\varepsilon(l, K_S\pi)$, %	5.70 ± 0.02	5.58 ± 0.02	5.95 ± 0.02	5.89 ± 0.02
$\mathcal{B}(K_S\pi\nu)$, %	0.406 ± 0.005	0.414 ± 0.005	0.397 ± 0.005	0.400 ± 0.005
$\langle\mathcal{B}\rangle_l$, %	0.410 ± 0.003		0.399 ± 0.003	
$\langle\mathcal{B}\rangle_{\rm all}$, %	0.404 ± 0.002			

Table 2
Systematic uncertainties

Source	Contribution, %
K_S detection efficiency	2.5
$\tau^+\tau^-$ background subtraction	1.6
$\sum E_\gamma^{\rm LAB}$	1.0
Lepton identification efficiency	0.8
Pion momentum	0.5
Non-$\tau^+\tau^-$ background subtraction	0.3
$\mathcal{B}(l\nu_l\nu_\tau)$	0.3
$\frac{\varepsilon(l_1,l_2)}{\varepsilon(l_1,K_S\pi)}$	0.2
K_S momentum	0.2
Pion identification efficiency	0.1
Total	3.3

where $N(l_1^\pm, K_S\pi^\mp)$, $\varepsilon(l_1^\pm, K_S\pi^\mp)$ are the number and MC efficiency of the signal $(l_1^\pm, K_S\pi^\mp)$ events, $N(l_1^\pm, l_2^\mp)$, $\varepsilon(l_1^\pm, l_2^\mp)$ are the number and MC efficiency of the two-lepton $(l_1^\pm, l_2^\mp)$ events, $\mathcal{B}(l_2^\mp\nu_l\nu_\tau)$ is the τ leptonic branching fraction taken from Ref. [20]. Note that the tag-lepton $(l_1^\pm)$ efficiency cancels in the ratio of the efficiencies, so the associated systematic uncertainty is reduced. The branching fractions calculated separately for each event configuration are given in Table 1, which also lists separately the averages for electrons and muons as well as the overall branching fraction.

Table 2 lists the different sources of systematic uncertainties for the branching fraction. The dominant contributions come from the K_S detection efficiency and background subtraction. A systematic uncertainty in the K_S detection efficiency receives contributions from the reconstruction of K_S daughter pions (2.3%), the efficiency for fitting two pion tracks to a common $\pi^+\pi^-$ vertex (0.9%), which was evaluated by varying the cut on the z-distance between the two helices at the vertex position before the fit, and the efficiency of the selection criteria (0.6%), which was checked by varying cuts on the $\pi^+\pi^-$ invariant mass $M_{\pi\pi}(K_S)$. Systematic uncertainties arising from $\tau^+\tau^-$-background subtraction are 0.8%, 1.1%, 0.6% and 0.5% for the $\tau^- \to K_S K_L \pi^-\nu_\tau$, $\tau^- \to K_S\pi^-\pi^0\nu_\tau$, $\tau^- \to K_S K^-\nu_\tau$ and $\tau^- \to \pi^-\pi^-\pi^+\nu_\tau$ modes, respectively. For the background from τ decay modes with a K_S the uncertainties are determined by the corresponding uncertainties in their branching fractions taken from Ref. [20], except for the $\tau^- \to K_S K_L \pi^-\nu_\tau$ mode. Here we rely on the isospin relation $\mathcal{B}(\tau^- \to K_S K_L \pi^-\nu_\tau) = 1/2\mathcal{B}(\tau^- \to K^+K^-\pi^-\nu_\tau)$ and the CLEO result [21] to calculate the $\tau^- \to K_S K_L \pi^-\nu$ branching fraction $\mathcal{B}(\tau^- \to K_S K_L \pi^-\nu_\tau) = (0.078 \pm 0.006)\%$. The uncertainty in the contamination by $\tau^- \to \pi^-\pi^-\pi^+\nu_\tau$ events is evaluated by varying the K_S decay length cut.

The lepton detection efficiency is corrected using the $e^+e^- \to e^+e^-l^+l^-$, $l = e, \mu$ two-photon data sample. An efficiency correction table is calculated in 70 bins on the plane of momentum vs polar angle in the laboratory frame and then applied to the Monte Carlo efficiencies $\varepsilon(l_1^\pm, K_S\pi^\mp)$ and $\varepsilon(l_1^\pm, l_2^\mp)$. Hence, the uncertainty on the leptonic efficiency is determined by the statistics of the $e^+e^- \to e^+e^-l^+l^-$ sample and the long-term stability, which is evaluated from the variation of the corrections calculated for time ordered subsamples of the experimental two-photon data. The pion identification efficiency in MC differs from that in data. In the signal sample, K_S mesons provide a source of identified pions, which are used to calculate corrections to the MC efficiency. Therefore, the systematic uncertainty on the pion identification efficiency is determined by the statistical error of the correction, which

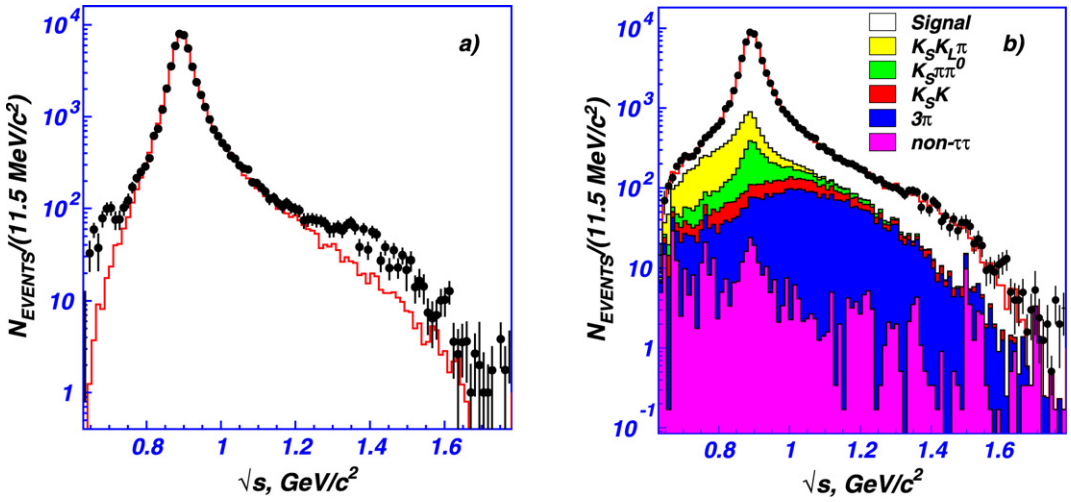

Fig. 3. Comparison of the $K_S\pi$ mass distributions, points are experimental data, histograms are spectra expected for different models. (a) Shows the fitted result with the model incorporating the $K^*(892)$ alone, here the background has been already subtracted from both experimental and expected distributions. (b) Shows the fitted result with the $K_0^*(800) + K^*(892) + K^*(1410)$ model, here different types of background are also shown.

is about 0.1%. To calculate $\varepsilon(l_1, K_S\pi)$ a signal MC sample is produced according to the $K^*(892) + K^*(1680)$ model and the model dependence of $\varepsilon(l_1, K_S\pi)$ is found to be negligible.

We also vary cuts on the pion momentum, the kaon momentum, and the total laboratory energy of photons ($\sum E_\gamma^{\rm LAB}$) to check the stability of the branching fraction. The total systematic uncertainty of 3.3% is obtained by adding all the contributions in quadrature. Our final result for the branching fraction is $\mathcal{B}(\tau^- \to K_S\pi^-\nu_\tau) = (0.404 \pm 0.002(\text{stat.}) \pm 0.013(\text{syst.}))\%$.

5. Analysis of the $\tau^- \to K_S\pi^-\nu_\tau$ spectrum

The $K_S\pi^-$ invariant mass distribution shown in Fig. 3 exhibits a very clear $K^*(892)^-$ signal. We parameterize this spectrum by the following function (see Ref. [8] for more detail):

$$\frac{d\Gamma}{d\sqrt{s}} \sim \frac{1}{s}\left(1 - \frac{s}{m_\tau^2}\right)^2\left(1 + 2\frac{s}{m_\tau^2}\right) \times P\left\{P^2|F_V|^2 + \frac{3(m_K^2 - m_\pi^2)^2}{4s(1 + 2\frac{s}{m_\tau^2})}|F_S|^2\right\}, \quad (2)$$

where s is the $K_S\pi^-$ invariant mass squared and P is the K_S momentum in the $K_S\pi^-$ rest frame:

$$P(s) = \frac{1}{2\sqrt{s}}\sqrt{\left[s - (m_K + m_\pi)^2\right]\left[s - (m_K - m_\pi)^2\right]}. \quad (3)$$

The vector form factor F_V is parameterized by the $K^*(892)$, $K^*(1410)$ and $K^*(1680)$ meson amplitudes:

$$F_V = \frac{1}{1 + \beta + \chi}\left[BW_{K^*(892)}(s) + \beta BW_{K^*(1410)}(s) + \chi BW_{K^*(1680)}(s)\right], \quad (4)$$

where β and χ are complex coefficients for the fractions of the $K^*(1410)$ and $K^*(1680)$ resonances, respectively. $BW_R(s)$, $(R = K^*(892),\ K^*(1410),\ K^*(1680))$ is a relativistic Breit–Wigner function:

$$BW_R(s) = \frac{M_R^2}{s - M_R^2 + i\sqrt{s}\Gamma_R(s)}, \quad (5)$$

where $\Gamma_R(s)$ is the s-dependent total width of the resonance:

$$\Gamma_R(s) = \Gamma_{0R}\frac{M_R^2}{s}\left(\frac{P(s)}{P(M_R^2)}\right)^{2\ell+1}, \quad (6)$$

where $\ell = 1(0)$ if the $K\pi$ system originates in the $P(S)$-wave state and Γ_{0R} is the resonance width at its peak.

The scalar form factor F_S includes the $K_0^*(800)$ and $K_0^*(1430)$ contributions, their fractions are described respectively by the complex constants $\varkappa$ and γ:

$$F_S = \varkappa\frac{s}{M^2_{K_0^*(800)}}BW_{K_0^*(800)}(s) + \gamma\frac{s}{M^2_{K_0^*(1430)}}BW_{K_0^*(1430)}(s). \quad (7)$$

The experimental distribution is approximated in the mass range from 0.63 GeV/c^2 to 1.78 GeV/c^2 by a function calculated from the convolution of the spectrum given by Eq. (2) and the detector response function, which takes into account the efficiency and finite resolution of the detector. In all fits the $K^*(892)$ mass and width as well as the total normalization are free parameters. Only the strengths (fractions) of the other K^*'s are free parameters, while their masses and widths are fixed at the world average values [20]. In the approximation $\varkappa$ is chosen to be real, because F_S is defined up to the common phase, which cancels in $|F_S|^2$.

Fig. 3(a) and Table 3 show that the $K^*(892)$ alone is not sufficient to describe the $K_S\pi$ mass spectrum. To describe the enhancement near threshold, we introduce a $K_0^*(800)$ amplitude, while for description of the distribution at higher invariant masses we try to include the $K^*(1410)$, $K^*(1680)$ vector resonances (see Table 3) or the scalar $K_0^*(1430)$ (see Table 4). Fig. 3(b) demonstrates the good quality of the fit with the

Table 3
Results of the fit of the $K_S\pi$ mass spectrum in different models of the non-$K^*(892)$ mechanism: the $K^*(1410)$ and $K^*(1680)$ contributions are described by the complex constants β and χ, respectively, while that from the $K_0^*(800)$ is described by the real constant $\varkappa$. Masses and widths of the non-$K^*(892)$ resonances were fixed at their PDG values (the $K_0^*(800)$ mass and width were fixed from Ref. [22])

	$K^*(892)$	$K_0^*(800)+K^*(892)+K^*(1410)$	$K_0^*(800)+K^*(892)+K^*(1680)$
$M_{K^*(892)^-}$, MeV/c^2	895.53 ± 0.19	895.47 ± 0.20	894.88 ± 0.20
$\Gamma_{K^*(892)^-}$, MeV	49.29 ± 0.46	46.19 ± 0.57	45.52 ± 0.51
$\lvert\beta\rvert$		0.075 ± 0.006	
$\arg(\beta)$		1.44 ± 0.15	
$\lvert\chi\rvert$			$0.117\pm{}^{0.017}_{0.033}$
$\arg(\chi)$			3.17 ± 0.47
$\varkappa$		1.57 ± 0.23	1.53 ± 0.24
χ^2/n.d.f.	448.4/87	90.2/84	106.8/84
$P(\chi^2)$, %	0	30	5

Table 4
Results of the fit of the $K_S\pi$ mass spectrum in the $K_0^*(800)+K^*(892)+K_0^*(1430)$ model (two solutions). The $K_0^*(1430)$ contribution is described by the complex constant γ, while that from the $K_0^*(800)$ is described by the real constant $\varkappa$. Masses and widths of the non-$K^*(892)$ resonances were fixed at their PDG values (the $K_0^*(800)$ mass and width were fixed from Ref. [22])

	$K_0^*(800)+K^*(892)+K_0^*(1430)$	
	Solution 1	Solution 2
$M_{K^*(892)^-}$, MeV/c^2	895.42 ± 0.19	895.50 ± 0.22
$\Gamma_{K^*(892)^-}$, MeV	46.14 ± 0.55	46.20 ± 0.69
$\lvert\gamma\rvert$	0.954 ± 0.081	1.92 ± 0.20
$\arg(\gamma)$	0.62 ± 0.34	4.03 ± 0.09
$\varkappa$	1.27 ± 0.22	2.28 ± 0.47
χ^2/n.d.f.	86.5/84	95.1/84
$P(\chi^2)$, %	41	19

Table 5
Results of the fit of the $K_S\pi$ mass spectrum in the model when the non-$K^*(892)$ mechanism is introduced by the LASS scalar form factor, described by the parameters a and b

	$K^*(892)+$LASS a, b-fixed	$K^*(892)+$LASS a, b-free
$M_{K^*(892)^-}$, MeV/c^2	895.42 ± 0.19	895.38 ± 0.23
$\Gamma_{K^*(892)^-}$, MeV	46.46 ± 0.47	46.53 ± 0.50
λ	0.282 ± 0.011	0.298 ± 0.012
a, $(\text{GeV}/c)^{-1}$	2.13 ± 0.10	$10.9\pm{}^{7.4}_{3.0}$
b, $(\text{GeV}/c)^{-1}$	3.96 ± 0.31	$19.0\pm{}^{4.5}_{3.6}$
χ^2/n.d.f.	196.9/86	97.3/83
$P(\chi^2)$, %	10^{-8}	13

$K_0^*(800)+K^*(892)+K^*(1410)$ model. It can be seen from Tables 3, 4 that we cannot distinguish between the $K_0^*(800)+K^*(892)+K^*(1410)$ and $K_0^*(800)+K^*(892)+K_0^*(1430)$ models. The fit quality with the $K_0^*(800)+K^*(892)+K^*(1680)$ model (see the fourth column of Table 3) is worse than that of the $K_0^*(800)+K^*(892)+K^*(1410)$ and $K_0^*(800)+K^*(892)+K_0^*(1430)$ models.

It should be noted that the absolute value of a sum of two Breit–Wigner functions of mass ($\sqrt{s}$) can have the same shape for two different sets of parameters. In the case of the $K_0^*(800)+K^*(892)+K_0^*(1430)$ model the relevant parameters are $\varkappa$, $|\gamma|$ and $\arg(\gamma)$. This statement holds true when mass-independent widths are considered. If the width is mass-dependent, some difference in the spectra appears. If in the fit to the data the errors are large enough, we cannot distinguish these solutions by their χ^2 values. For high statistics the two solutions can be distinguished by a χ^2 test. While for the $K_0^*(800)+K^*(892)+K^*(1410)$ and $K_0^*(800)+K^*(892)+K^*(1680)$ models with a complicated vector form factor the values of χ^2 are significantly different (due to the small ($\sim 1\%$) errors at the $K^*(892)$ peak), in the $K_0^*(800)+K^*(892)+K_0^*(1430)$ case with a complicated scalar form factor different solutions result in similar $P(\chi^2)$ values (see Table 4) due to the relatively low statistics in the region of the $K_0^*(800)$ and $K_0^*(1430)$ peaks.

An alternative way to describe our data is to use the parameterization of the scalar form factor suggested by the LASS experiment [23,24]:

$$F_S = \lambda A_{\text{LASS}}(s),$$
$$A_{\text{LASS}} = \frac{\sqrt{s}}{P}\left(\sin\delta_B e^{i\delta_B} + e^{2i\delta_B} B W_{K_0^*(1430)}(s)\right), \quad (8)$$

where λ is a real constant, P is K_S momentum in the $K_S\pi$ rest frame (see Eq. (3)), and the phase δ_B is determined from the equation $\cot\delta_B = \frac{1}{aP} + \frac{bP}{2}$, where a, b are the model parameters. In this parameterization the non-resonant mechanism is given by the effective range term $\sin\delta_B e^{i\delta_B}$, while the resonant structure is described by the $K_0^*(1430)$ amplitude.

Table 5 shows the results of fits to the spectrum in models, where the non-$K^*(892)$ mechanism is described by the LASS parameterization of the scalar form factor. In the first fit (see the second column of Table 5) a and b parameters were fixed at the LASS optimal values [24]. In the second fit a and b were free parameters (see the third column of Table 5). The optimal values of a and b in our fit differ significantly from the values obtained by the LASS Collaboration in experiments on $K\pi$ scattering [23].

The $K_0^*(800)+K^*(892)+K^*(1410)$ model was considered as the default and was used to obtain the $K^*(892)(K_S\pi)\nu$ fraction in the $K_S\pi\nu$ final state, which was found to be $\mathcal{B}(\tau^-\to K^*(892)^-\nu_\tau)\cdot\mathcal{B}(K^*(892)^-\to K_S\pi^-)/\mathcal{B}(\tau^-\to K_S\pi^-\nu_\tau) = 0.933\pm0.027$. The 0.027 error includes the model uncertainty,

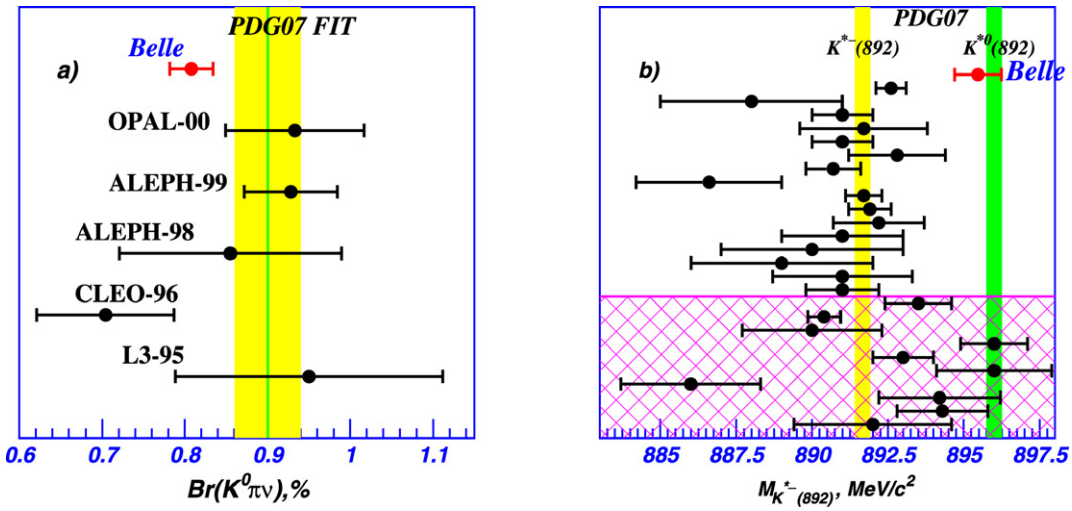

Fig. 4. Comparison of the $\tau^- \to \bar{K}^0\pi^-\nu_\tau$ branching fraction (a) and $K^*(892)^-$ mass (b) measured in different experiments. (b) Also shows all available data on the $K^*(892)^-$ mass together with the PDG average (the hatched region marks PDG data, which were not used in the calculation of the average mass, see Ref. [20]), as well as our result, which is close to the PDG $K^*(892)^0$ mass.

which was found by calculating this fraction in the fits with the other models mentioned above, as well as the uncertainty in the fit parameters. Finally we obtain $\mathcal{B}(\tau^- \to K^*(892)^-\nu_\tau) \cdot \mathcal{B}(K^*(892)^- \to K_S\pi^-) = (3.77 \pm 0.02(\text{stat.}) \pm 0.12(\text{syst.}) \pm 0.12(\text{mod.})) \times 10^{-3}$.

6. Measurement of the $K^*(892)^-$ mass and width

A fit to the $K_S\pi^-$ invariant mass spectrum also provides a high precision measurement of the $K^*(892)^-$ mass and width. We consider a fit with the $K_0^*(800) + K^*(892) + K^*(1410)$ model, which provides a good description of the data, as a reference, and use it to obtain the $K^*(892)^-$ mass and width values. It can be seen from Table 3 that the statistical uncertainty is about 0.20 MeV/c^2 for the mass and 0.6 MeV for the width. Two additional sources of uncertainty are studied: the effects of imperfect knowledge of the detector response function and model uncertainty.

The systematic uncertainty is studied with a MC sample by comparing the $K^*(892)^-$ parameters implemented in the generator and its parameters after the full reconstruction procedure (the detector response function is determined from other statistically independent MC simulations of signal events). It is found to be 0.44 MeV/c^2 for the mass and 1.0 MeV for the width.

The model uncertainty is investigated by fitting the $K_S\pi^-$ mass spectrum with different models. The maximal difference from the reference value is considered as a model uncertainty. It is found to be 0.59 MeV/c^2 for the mass and 0.7 MeV for the width.

As a result, the $K^*(892)^-$ mass and width are $M(K^*(892)^-) = (895.47 \pm 0.20(\text{stat.}) \pm 0.44(\text{syst.}) \pm 0.59(\text{mod.}))$ MeV/c^2 and $\Gamma(K^*(892)^-) = (46.2 \pm 0.6(\text{stat.}) \pm 1.0(\text{syst.}) \pm 0.7(\text{mod.}))$ MeV, where the first uncertainty is statistical, the second is systematic and the third is from the model.

7. Conclusions

The branching fraction of the $\tau^- \to K_S\pi^-\nu_\tau$ decay has been measured using a data sample of 351.4 fb^{-1} collected with the Belle detector. Our result is:

$$\mathcal{B}(\tau^- \to K_S\pi^-\nu_\tau) = \big(0.404 \pm 0.002(\text{stat.}) \pm 0.013(\text{syst.})\big)\%.$$

To compare our result with the previous measurements made by the OPAL [27], ALEPH [10,28], CLEO [11] and L3 [29] groups we calculate the $\tau^- \to \bar{K}^0\pi^-\nu_\tau$ branching fraction according to the formula $\mathcal{B}(\tau^- \to \bar{K}^0\pi^-\nu_\tau) = \mathcal{B}(\tau^- \to K_S\pi^-\nu_\tau) + \mathcal{B}(\tau^- \to K_L\pi^-\nu_\tau) = 2\mathcal{B}(\tau^- \to K_S\pi^-\nu_\tau)$ and obtain:

$$\mathcal{B}(\tau^- \to \bar{K}^0\pi^-\nu_\tau) = \big(0.808 \pm 0.004(\text{stat.}) \pm 0.026(\text{syst.})\big)\%.$$

Fig. 4(a) shows the results of various measurements of the $\tau^- \to \bar{K}^0\pi^-\nu_\tau$ branching fraction, along with the Particle Data Group (PDG) fit value ($\mathcal{B}_{\text{PDG}}(\tau^- \to \bar{K}^0\pi^-\nu_\tau) = (0.900 \pm 0.040)\%$) [20] and our result. Our result is consistent with previous measurements, but is more precise.

The $K^*(892)$ alone is not sufficient to describe the $K_S\pi$ invariant mass spectrum. The best description is achieved in the $K_0^*(800) + K^*(892) + K^*(1410)$ and $K_0^*(800) + K^*(892) + K_0^*(1430)$ models. Future high precision studies of the invariant mass spectra in τ lepton decays with kaons combined with angular analysis, i.e., an application of the structure function formalism suggested in Ref. [1], will elucidate the nature of the scalar form factor. They will also check various theoretical models describing the scalar $K\pi$ sector, e.g., the predictions of the resonance chiral theory [25] and the parameters of the $K_0^*(800)$ resonance calculated from the Roy–Steiner representations in a model-independent way [26].

The product of $\tau^- \to K^*(892)^-\nu_\tau$ and $K^*(892)^- \to K_S\pi^-$ branching fractions is found to be:

$$\mathcal{B}\big(\tau^- \to K^*(892)^-\nu_\tau\big) \cdot \mathcal{B}\big(K^*(892)^- \to K_S\pi^-\big) = \big(3.77 \pm 0.02(\text{stat.}) \pm 0.12(\text{syst.}) \pm 0.12(\text{mod.})\big) \times 10^{-3},$$

also the $K^*(892)^-$ mass and width are measured:

$$M\left(K^*(892)^-\right) = \left(895.47 \pm 0.20(\text{stat.}) \pm 0.44(\text{syst.}) \pm 0.59(\text{mod.})\right) \text{MeV}/c^2,$$
$$\Gamma\left(K^*(892)^-\right) = \left(46.2 \pm 0.6(\text{stat.}) \pm 1.0(\text{syst.}) \pm 0.7(\text{mod.})\right) \text{MeV}.$$

The values of the $K^*(892)^-$ mass and width that we obtain are more precise than any of the existing measurements of these quantities listed in Ref. [20] and shown in Fig. 4(b). While our determination of the width is compatible with most of the previous measurements within experimental errors, our mass value is systematically higher than those before and is in fact consistent with the world average value of the neutral $K^*(892)^0$ mass, which is (896.00 ± 0.25) MeV/c^2 [20]. Note that all earlier mass measurements listed in Ref. [20] come from analysis of hadronic reactions and include the effects of final state interaction while our work presents a measurement based on τ^- decays, where the decay products of the $K^*(892)^-$ are the only hadrons involved. It is also noteworthy that none of the previous measurements in Ref. [20], all of which were performed more than 20 years ago, present the systematic uncertainties for their measurements. Unfortunately, previous studies of the $K^*(892)^-$ in τ^- lepton decays usually do not determine its parameters. The only published result we are aware of is that of ALEPH [30], which is consistent with ours. Its accuracy, however, is much worse and no systematic errors are presented, which precludes any detailed comparisons. A similar $K^*(892)^-$ mass shift of $(+4.7 \pm 0.9)$ MeV/c^2 was reported by CLEO [31], but no dedicated study of this effect was published. Future dedicated measurements of the $K^*(892)^-$ parameters with high precision are necessary to clarify this discrepancy and shed light on the long standing issue of the electromagnetic mass difference between the charged and neutral $K^*(892)$ [32,33].

Acknowledgements

We are grateful to M. Jamin for interesting discussions. We thank the KEKB group for the excellent operation of the accelerator, the KEK cryogenics group for the efficient operation of the solenoid, and the KEK computer group and the National Institute of Informatics for valuable computing and Super-SINET network support. We acknowledge support from the Ministry of Education, Culture, Sports, Science, and Technology of Japan and the Japan Society for the Promotion of Science; the Australian Research Council and the Australian Department of Education, Science and Training; the National Science Foundation of China and the Knowledge Innovation Program of the Chinese Academy of Sciences under contract No. 10575109 and IHEP-U-503; the Department of Science and Technology of India; the BK21 program of the Ministry of Education of Korea, the CHEP SRC program and Basic Research program (grant No. R01-2005-000-10089-0) of the Korea Science and Engineering Foundation, and the Pure Basic Research Group program of the Korea Research Foundation; the Polish State Committee for Scientific Research; the Ministry of Education and Science of the Russian Federation and the Russian Federal Agency for Atomic Energy; the Slovenian Research Agency; the Swiss National Science Foundation; the National Science Council and the Ministry of Education of Taiwan; and the US Department of Energy.

References

[1] J.H. Kühn, E. Mirkes, Z. Phys. C 56 (1992) 661; J.H. Kühn, E. Mirkes, Z. Phys. C 67 (1995) 364, Erratum.
[2] R. Decker, E. Mirkes, R. Sauer, Z. Wąs, Z. Phys. C 58 (1993) 445.
[3] M. Finkemeier, E. Mirkes, Z. Phys. C 69 (1996) 243.
[4] E. Gamiz, et al., Phys. Rev. Lett. 94 (2005) 011803.
[5] J. Dorfan, et al., MARK II Collaboration, Phys. Rev. Lett. 46 (1981) 215.
[6] H. Albrecht, et al., ARGUS Collaboration, Z. Phys. C 41 (1988) 1.
[7] M. Battle, et al., CLEO Collaboration, Phys. Rev. Lett. 73 (1994) 1079.
[8] M. Finkemeier, E. Mirkes, Z. Phys. C 72 (1996) 619.
[9] J.J. Godina Nava, G. Lopez Castro, Phys. Rev. D 52 (1995) 2850.
[10] R. Barate, et al., ALEPH Collaboration, Eur. Phys. J. C 10 (1999) 1.
[11] T.E. Coan, et al., CLEO Collaboration, Phys. Rev. D 53 (1996) 6037.
[12] S. Kurokawa, E. Kikutani, Nucl. Instrum. Methods A 499 (2003) 1, and other papers included in this volume.
[13] Z. Natkaniec, et al., Belle SVD2 Group, Nucl. Instrum. Methods A 560 (2006) 1.
[14] A. Abashian, et al., Belle Collaboration, Nucl. Instrum. Methods A 479 (2002) 117.
[15] K. Hanagaki, et al., Nucl. Instrum. Methods A 485 (2002) 490.
[16] A. Abashian, et al., Nucl. Instrum. Methods A 491 (2002) 69.
[17] S. Jadach, Z. Wąs, Comput. Phys. Commun. 85 (1995) 453.
[18] Z. Wąs, Nucl. Phys. B (Proc. Suppl.) 98 (2001) 96.
[19] R. Brun et al., GEANT 3.21, CERN Report No. DD/EE/84-1 (1984).
[20] W.-M. Yao, et al., J. Phys. G 33 (2006) 1.
[21] R.A. Briere, et al., CLEO Collaboration, Phys. Rev. Lett. 90 (2003) 181802.
[22] M. Ablikim, et al., BES Collaboration, Phys. Lett. B 633 (2006) 681.
[23] D. Aston, et al., LASS Collaboration, Nucl. Phys. B 296 (1988) 493.
[24] B. Aubert, et al., BaBar Collaboration, Phys. Rev. D 72 (2005) 072003.
[25] M. Jamin, A. Pich, J. Portoles, Phys. Lett. B 640 (2006) 176.
[26] S. Descotes-Genon, B. Moussallam, Eur. Phys. J. C 48 (2006) 553.
[27] G. Abbiendi, et al., OPAL Collaboration, Eur. Phys. J. C 13 (2000) 213.
[28] R. Barate, et al., ALEPH Collaboration, Eur. Phys. J. 4 (1998) 29.
[29] M. Acciarri, et al., L3 Collaboration, Phys. Lett. B 345 (1995) 93.
[30] R. Barate, et al., ALEPH Collaboration, Eur. Phys. J. C 11 (1999) 599.
[31] G. Bonvicini, et al., CLEO Collaboration, Phys. Rev. Lett. 88 (2002) 111803.
[32] A. De Rujula, H. Georgi, S.L. Glashow, Phys. Rev. D 12 (1975) 147.
[33] M. Aguilar-Benitez, et al., HBC Collaboration, Nucl. Phys. B 141 (1978) 101.